

Article

High-Temperature Raman Spectroscopy of Nano-Crystalline Carbon in Silicon Oxycarbide

Felix Rosenburg ^{*}, Emanuel Ionescu , Norbert Nicoloso and Ralf Riedel

Institut für Material- und Geowissenschaften, Technische Universität Darmstadt, Otto-Berndt-Straße 3, 64287 Darmstadt, Germany; ionescu@materials.tu-darmstadt.de (E.I.); nn@eurad.com (N.N.); riedel@materials.tu-darmstadt.de (R.R.)

* Correspondence: rosenburg@materials.tu-darmstadt.de; Tel.: +49-6151-1621622

Received: 5 December 2017; Accepted: 5 January 2018; Published: 9 January 2018

Abstract: The microstructure of segregated carbon in silicon oxycarbide (SiOC), hot-pressed at $T = 1600$ °C and $p = 50$ MPa, has been investigated by VIS Raman spectroscopy ($\lambda = 514$ nm) within the temperature range 25–1000 °C in air. The occurrence of the G, D' and D bands at 1590, 1620 and 1350 cm^{-1} , together with a lateral crystal size $L_a < 10$ nm and an average distance between lattice defects $L_D \approx 8$ nm, provides evidence that carbon exists as nano-crystalline phase in SiOC containing 11 and 17 vol % carbon. Both samples show a linear red shift of the G band up to the highest temperature applied, which is in agreement with the description of the anharmonic contribution to the lattice potential by the modified Tersoff potential. The temperature coefficient $\chi_G = -0.024 \pm 0.001$ $\text{cm}^{-1}/\text{°C}$ is close to that of disordered carbon, e.g., carbon nanowalls or commercial activated graphite. The line width of the G band is independent of temperature with FWHM-values of 35 cm^{-1} (C-11) and 45 cm^{-1} (C-17), suggesting that scattering with defects and impurities outweighs the phonon-phonon and phonon-electron interactions. Analysis of the Raman line intensities indicates vacancies as dominating defects.

Keywords: polymer-derived ceramics; Raman spectroscopy; anharmonicity; carbon; defects

1. Introduction

Phonons are of fundamental importance for crystalline materials. The analysis of Raman active modes is well-suited to assessing the lattice dynamics of, e.g., carbon and its allotropes graphite [1,2], carbon nanotubes, [3–5] graphene, [6,7] amorphous carbon, [8,9] and diamond-like carbon [10,11]. It is very sensitive to the hybridization state of carbon, and provides information about the microstructure and properties such as the thermal conductivity, the specific heat and the thermal expansion [12].

In this work, we present a temperature-dependent Raman study of silicon oxycarbide (SiOC) containing 11 and 17 vol % of segregated carbon (labeled as C-11 and C-17 in the following). Amorphous SiO₂ and fine dispersed carbon are the main constituents of these ceramic nano-composites [13]. Due to its unique microstructure, SiOC possesses a variety of interesting properties, such as high temperature and corrosion stability [14–16], high creep resistance [17] and high piezoresistivity [18,19]. Furthermore, SiOC-based materials have been shown to exhibit promising behavior as anode materials in Li-ion batteries [20]. Interestingly, the mentioned properties seem to be determined by the segregated carbon phase randomly distributed within the SiOC matrix. Depending on the concentration of carbon and the synthesis conditions, different carbon structures can be observed, as shown, e.g., in ref. [21]. At low concentrations and low pyrolysis temperatures ($T < 1000$ °C), highly disordered carbon domains embedded in an insulating SiOC matrix exist. At volume fractions larger than ≈ 5 vol % and synthesis temperatures beyond 1400 °C, a randomly grown continuous carbon network is formed [22]. Accordingly, C-11 and C-17 represent samples with

concentrations well beyond the percolation threshold, ensuring that their properties solely depend on the state of the carbon within the composite material.

As mentioned above, the segregated carbon in silicon oxycarbide-based materials seems to determine many of its properties. As some of those are present or may be used at high temperatures (e.g., near-zero creep or piezoresistive behavior), it seems appropriate to study the nature and the temperature-dependent evolution of the segregated carbon phase in SiOC materials at high temperatures. Thus, the aim of the present study was to investigate the temperature evolution of the segregated carbon in SiOC by using Raman spectroscopy.

At ambient pressure, the thermal investigation of carbon is restricted to temperatures up to about 600 °C where carbon starts to oxidize. The segregated carbon in C-11 and C-17, on the contrary, is covered by silica, which protects it from oxidation, thus allowing investigations at significantly higher temperatures. In case of reducing conditions, e.g., under Ar/H₂, in-situ Raman investigations are possible at even higher temperatures. Montagnac et al. recorded the Raman data of pyrolytic graphite (PG) and highly orientated pyrolytic graphite (HOPG) up to temperatures of about 2400 °C [23]. To our knowledge, no other carbon allotropes have been investigated up to such high temperatures, and no investigations higher than 600 °C have been performed in air.

Within the allowed phonon modes of crystalline carbon only the E_{2g} mode (G band) is Raman active. The thermodynamic derivation of its frequency change $\Delta\omega$ with temperature T , volume V and pressure p is described by [12]:

$$\Delta\omega = (\chi_T + \chi_V)\Delta T = \left(\frac{d\omega}{dT}\right)_V \Delta T + \left(\frac{d\omega}{dV}\right)_T \Delta V = \left(\frac{d\omega}{dT}\right)_V \Delta T + \left(\frac{d\omega}{dV}\right)_T \left(\frac{dV}{dT}\right)_p \Delta T \quad (1)$$

with χ_T the intrinsic temperature effect due to the direct coupling of phonon modes and χ_V the volume effect due to the thermal expansion. The thermal expansion of the graphite crystal occurs mainly along the c -axis perpendicular to the graphene layers of its hexagonal structure (space group: P6₃mc), resulting in a small effect on the in-plane E_{2g} mode. Hence, Equation (1) can be reduced to:

$$\Delta\omega = \chi_T \cdot \Delta T \quad (2)$$

According to Equation (2), the G line shifts linearly with temperature, only few works report a non-linear shift [24,25].

It is well known that the temperature dependence of the phonon dispersion curves of carbon materials is a direct consequence of anharmonic contributions to the lattice potential [26]. According to the molecular dynamics simulation (MD) of Koukaras et al., each of the inserted potentials produces a good description of some phonon branches but none works for all of the optical and acoustical branches of graphene [12,27]. However, the modified Tersoff potential [28] correctly describes the temperature dependence of the E_{2g} mode (Raman G band). A linear down-shift of the G line or softening of the E_{2g} mode, respectively, is predicted within the temperature range investigated (−200 to 1200 °C). Since the G band is associated with the in-plane vibration in sp² carbon, the shift with temperature should be similar for the various carbon materials, i.e., we expect a linear dependence for carbon enclosed in the SiOC matrix with a temperature coefficient χ_G of about −0.02 cm^{−1}/°C, as experimentally observed in graphene [12,29] HOPG [30] and SWNTs [31–33] at low temperatures ($T < 600$ °C).

2. Materials and Methods

In order to synthesize polymer-derived SiOC ceramics, commercially available preceramic polymer resins of the companies Starfire Systems Ltd. (Glenville, NY, USA) (Polyramic[®]: SPR 212) and Wacker Chemie AG (München, Germany) (BELSIL[®] PMS-MK) have been used. The preceramic polymers were thermally crosslinked in an alumina tube furnace at $T = 250$ °C for 2 h and subsequently pyrolyzed at $T = 1100$ °C for 2 h with a heating and cooling rate of 100 °C/h under a constant argon

flow (5 L/h). To ensure an oxygen-free atmosphere during calcination, the chamber was evacuated several times and purged with high purity argon. The resulting black glass was milled and sieved to a particle size below $\leq 40 \mu\text{m}$. Subsequently, the powder was sealed within graphite foils and hot-pressed using the spark plasma sintering technology without any sinter additives at $T = 1600 \text{ }^\circ\text{C}$ with a uniaxial load of $p = 50 \text{ MPa}$ for 15 min under high purity argon atmosphere and a heating rate of $320 \text{ }^\circ\text{C}/\text{min}$. After the pressure-assisted sintering process, black dense monoliths were obtained and cut into cylindrical shape ($d = 5 \text{ mm}$) using a grinding machine equipped with a diamond grinding wheel.

Raman spectra were collected using a Renishaw InVia Raman microscope equipped with an Ar laser ($\lambda = 514.5 \text{ nm}$). The measurements were performed by using a grating of $600 \text{ g}\cdot\text{mm}^{-1}$ and a confocal microscope (magnification $100\times$ NA 0.9) with a $100 \mu\text{m}$ aperture and a lateral resolution of $2\text{--}4 \mu\text{m}$. The spectra were recorded in the wavenumber region of $400\text{--}3100 \text{ cm}^{-1}$ with a resolution of $<1 \text{ cm}^{-1}$ at RT and $<3 \text{ cm}^{-1}$ at $1000 \text{ }^\circ\text{C}$. The laser power (20 mW) was attenuated by using neutral density filters; thus, the power on the sample was in the range from $6 \mu\text{W}$ to 2 mW . In-situ heating of the samples was performed using a TS1500 heating stage from Linkam with a heating rate of $100 \text{ }^\circ\text{C}/\text{min}$ up to $T = 1000 \text{ }^\circ\text{C}$.

3. Results and Discussion

Figure 1 shows a typical room-temperature Raman spectrum of a C-11 sample synthesized at $T = 1600 \text{ }^\circ\text{C}$ with the D band at 1350 cm^{-1} , the G band at 1590 cm^{-1} and the D' band at 1620 cm^{-1} . The D band is induced by any kind of disorder. It is forbidden in graphite, but becomes Raman active through a disorder-induced double resonance Raman process [34,35], which causes in-plane breathing vibrations of the aromatic ring structures (A_{1g} symmetry). The D' band is also a disorder-induced double resonance process and is often found in nano-crystalline graphite [36,37]. The G band is assigned to the in-plane stretching vibration of sp^2 carbon (E_{2g} symmetry). Two additional features are observed at 2700 and 2900 cm^{-1} labeled as the 2D band (an overtone of the D band) and the D + G band (a combination of the D and G band) [6,38].

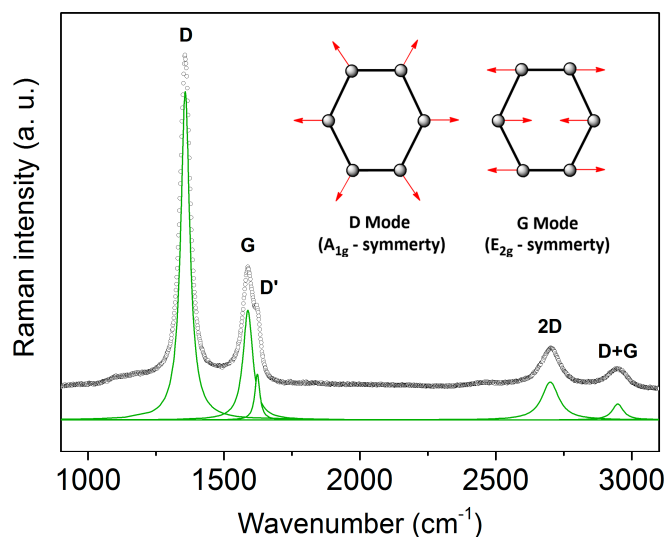


Figure 1. Room-temperature Raman spectrum of C-11. Green line: Lorentzian fits to the Raman modes. The inset shows the vibration modes of the D and G band.

The presence of both the G and D' band in the C-11 (and C-17) spectra indicates nano-crystalline carbon. The values of the lateral crystal size (L_a) and of the average distance between lattice defects (L_D) provide further evidence for this kind of carbon. According to Cançado et al.

$$L_a = (2.4 \times 10^{-10}) \cdot \lambda_L^4 \cdot \left(\frac{A_D}{A_G}\right)^{-1} \quad (3)$$

with λ_L the wavelength of the laser and A_D and A_G the area of the D and G band [39]. From Equation (3), an average lateral crystal size of $L_a \approx 10$ nm can be derived for C-11 and C-17.

The graphitization of diamond-like carbon within the temperature range of 1800–2700 °C has been investigated by Cañado et al. [39]. The lateral crystal size strongly increases from ≈ 20 nm (1800 °C) to ≈ 500 nm (2700 °C). As shown in Figure 2, the L_a values for C-11 and C-17, typically about 10 nm within $1200 < T < 1600$ °C, join at the onset of graphite formation, further supporting the assignment to nano-crystalline carbon.

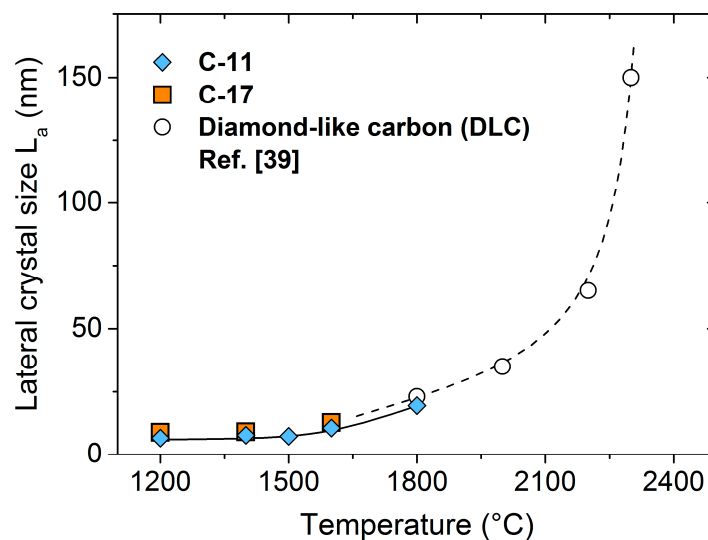


Figure 2. Lateral crystal size L_a of carbon as a function of the temperature. Open points: Adapted from ref. [39], dashed line: guideline for the eye.

The phonon dispersion curves of nano-crystalline carbon are expected to be different from that of well-ordered carbon (HOPG, graphene) due to the different microstructure and the presence of defects and impurities. Their influence can be followed by the investigation of the thermal shift of the G band of the different carbon structures. Figure 3a presents the Raman spectra of C-11 within the temperature range 25–1000 °C. A linear shift to lower frequencies occurs for all modes G, D and D'.

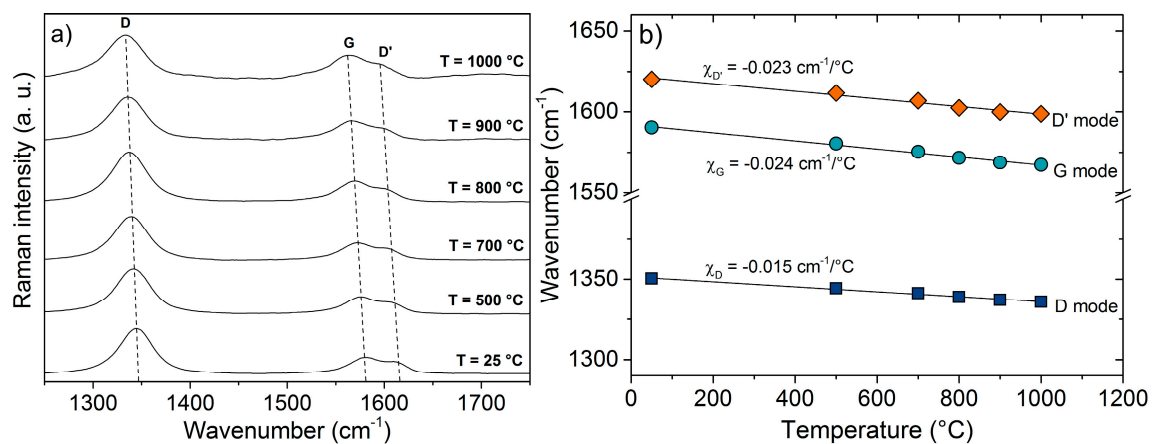


Figure 3. Temperature-dependent Raman spectra (a) and thermal coefficients of the Raman bands (b) of C-11.

The shift to a lower wavelength of the G mode with temperature results from an anharmonic contribution to the lattice potential and verifies the results of the MD simulation by Koukaras et al. [27] using the Tersoff potential modified by Lindsay and Broido [28].

The thermal coefficients χ , see Equation (2), are depicted in Figure 3b for the sample C-11. Very similar shifts are seen for C-17. The obtained values for the G band of C-11 ($\chi_G = -0.024 \text{ cm}^{-1}/^\circ\text{C}$) and C-17 ($\chi_G = -0.023 \text{ cm}^{-1}/^\circ\text{C}$) are significantly larger than that for well-ordered graphene ($\chi_G = -0.016 \text{ cm}^{-1}/^\circ\text{C}$) and HOPG ($\chi_G = -0.011 \text{ cm}^{-1}/^\circ\text{C}$), but smaller than the values for carbon nanowalls (CNWs) [40] and commercial activated graphite [41]: $\chi_G = -0.029 \text{ cm}^{-1}/^\circ\text{C}$ and $\chi_G = -0.027 \text{ cm}^{-1}/^\circ\text{C}$, respectively. Thus, as in activated graphite, defects and impurities appear to be decisive for the temperature dependence of the Raman G band. Table 1 summarizes the thermal coefficients χ_G of the different carbon materials.

Table 1. Temperature coefficients of carbon-based materials.

Sample	$\chi_G \text{ (cm}^{-1}/^\circ\text{C)}$	Temperature Range ($^\circ\text{C}$)	Reference
graphene	-0.016	-200–100	[12]
HOPG	-0.011	10–370	[41]
C-17	-0.023	25–1000	this work
C-11	-0.024	25–1000	this work
activated C	-0.027	150–500	[42]
CNW	-0.029	25–600	[40]

The thermal coefficients of the D and D' band in C-11 and C-17 ($\chi_D = -0.015$ and $\chi_{D'} = -0.023 \text{ cm}^{-1}/^\circ\text{C}$) match the values observed for CNTs ($\chi_D = -0.014$ and $\chi_{D'} = -0.015\text{--}0.020 \text{ cm}^{-1}/^\circ\text{C}$) [33] containing a significant amount of impurities.

Apart from the G shift, information about the phonon properties can be obtained from the width of the G line. Figure 4 shows the temperature dependence of the G-line width of C-11 and C-17. The full width at half maximum (FWHM) of both samples is temperature independent, with values of 35 cm^{-1} and 45 cm^{-1} . The error bars indicate the standard deviation of the FWHM values. Due to thermal radiation, the error significantly increases with temperature. Theoretical data for graphite and graphene yield a FWHM of $\approx 12 \text{ cm}^{-1}$, which decreases with increasing temperature above $T > 25 \text{ }^\circ\text{C}$ due to phonon-phonon interaction [43]. Experimental data for HOPG provide a FWHM of $\approx 15 \text{ cm}^{-1}$ independent of temperature (up to $\approx 700 \text{ }^\circ\text{C}$), [23] suggesting that the phonon-phonon interaction is compensated by phonon-electron interactions (which typically increase with temperature) [23]. In comparison to these well-ordered carbon materials, the significantly larger FWHM of nano-crystalline C-11 and C-17 cannot be solely explained by phonon-phonon and phonon-electron interactions; scattering with defects and impurities most likely determines the line width of the G band in these less-ordered materials.

The G and D' bands of nano-crystalline carbon in C-11 and C-17 seem to be correlated, since very similar constant ratios of the line widths of the G and D' bands are observed. The ratio $\text{FWHM}_G(\text{C-11})/\text{FWHM}_G(\text{C-17})$ accounts to 0.77 and $\text{FWHM}_{D'}(\text{C-11})/\text{FWHM}_{D'}(\text{C-17})$ is 0.82, respectively. The close correspondence suggests that probably one type of defect in the nano-crystalline structure defines the phonon lifetimes τ ($\tau \sim \text{FWHM}^{-1}$) of the G and D' band. C-17 contains carbon and defect concentrations higher than those of C-11. Supposing that scattering with the defects determines the phonon properties in a similar fashion, the FWHM of both lines will increase with the defect concentration. At the same time, the ratio between FWHM and defect concentration remains constant, as indicated by the experiment.

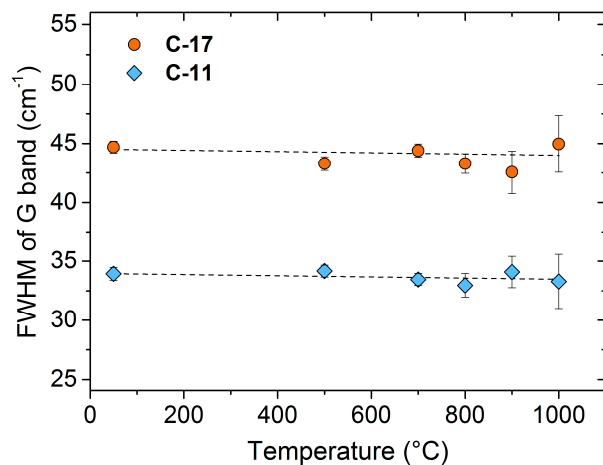


Figure 4. Temperature dependence of the FWHM of the G band of C-11 and C-17.

Information about the type of defects in carbon can be derived from the intensity ratios of the D, D' and G bands. A systematic study of the defects in graphene and graphite has been performed by Eckmann et al. [44]. By plotting the intensity ratio I_D/I_G versus $I_{D'}/I_G$, different types of defects can be distinguished by the respective slopes (sp^3 : ≈ 13 , vacancies: ≈ 7 and boundaries: ≈ 3.5). Figure 5 compares C-11 and C-17 with graphite and modified graphene. C-11 and C-17 fit into the I_D/I_G versus $I_{D'}/I_G$ —dependency observed for vacancies, suggesting that this type of defect dominates the phonon characteristics of nano-crystalline carbon in the silicon oxycarbide ceramics.

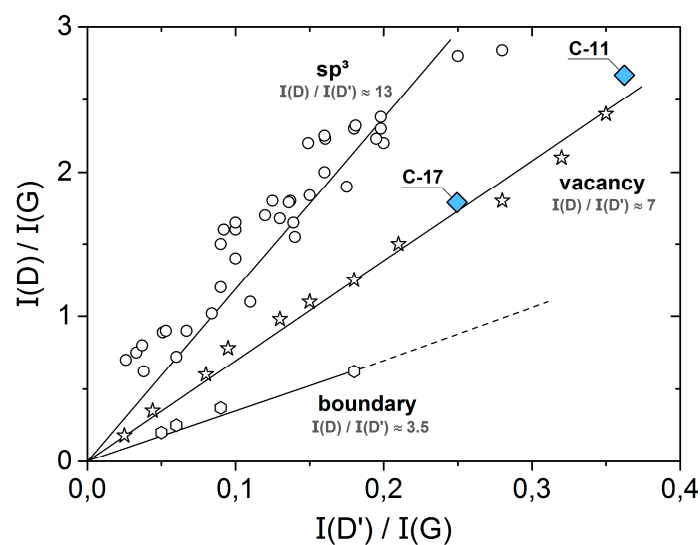


Figure 5. I_D/I_G versus $I_{D'}/I_G$ -plot. Open symbols: ref. [44].

4. Conclusions

In summary, we report on the Raman data of nano-crystalline carbon in SiOC containing 11 and 17 vol % carbon (samples C-11 and C-17) in the temperature range of 25–1000 °C. The temperature coefficient of the Raman G band is $\chi_G = -0.024 \pm 0.001 \text{ cm}^{-1}/^\circ\text{C}$ for both samples, very similar to that of disordered carbon materials, e.g., commercial activated graphite or carbon nanowalls. The observed linear temperature dependence of the G mode up to 1000 °C agrees with the description of the anharmonicity in the lattice potential by the modified Tersoff potential. The line width of the G (and D') band is temperature independent and significantly larger than that of well-ordered HOPG or graphene

indicating that the phonon characteristics are mainly determined by the interaction with defects and impurities. According to the Raman analysis, vacancies are predominant within the nano-crystalline carbon lattice.

Acknowledgments: The authors gratefully acknowledge financial support by the Deutsche Forschungsgemeinschaft (DFG, Ri 510/52-1 and IO 64/9-1). Daniel Wett (University of Chemnitz) is acknowledged for assistance with the Raman measurements.

Author Contributions: F.R., N.N., E.I. and R.R. conceived and designed the experiments; F.R. performed the experiments. F.R. and N.N. analyzed the data and wrote the manuscript. All authors read the paper and provided input and corrections on the text.

Conflicts of Interest: The authors declare no conflict of interest.

References

1. Ferrari, A.C. Raman spectroscopy of graphene and graphite: Disorder, electron-phonon coupling, doping and nonadiabatic effects. *Solid State Commun.* **2007**, *143*, 47–57. [[CrossRef](#)]
2. Tuinstra, F.; Koenig, J.L. Raman Spectrum of Graphite. *J. Chem. Phys.* **1970**, *53*, 1126–1130. [[CrossRef](#)]
3. Tessonier, J.-P.; Rosenthal, D.; Hansen, T.W.; Hess, C.; Schuster, M.E.; Blume, R.; Girgsdies, F.; Pfänder, N.; Timpe, O.; ShengSu, D. Analysis of the structure and chemical properties of some commercial carbon nanostructures. *Carbon* **2009**, *47*, 1779–1798. [[CrossRef](#)]
4. Dresselhaus, M.S.; Dresselhaus, G.; Jorio, A.; Filho, A.G.S.; Saitof, R. Raman spectroscopy on isolated single wall carbon nanotubes. *Carbon* **2002**, *40*, 2043–2061. [[CrossRef](#)]
5. Dresselhaus, M.S.; Dresselhaus, G.; Saito, R.; Joriod, A. Raman spectroscopy of carbon nanotubes. *Phys. Rep.* **2005**, *409*, 47–99. [[CrossRef](#)]
6. Ferrari, A.C.; Basko, D.M. Raman spectroscopy as a versatile tool for studying the properties of graphene. *Nat. Nanotechnol.* **2013**, *8*, 235–246. [[CrossRef](#)] [[PubMed](#)]
7. Malard, L.M.; Pimenta, M.A.; Dresselhaus, G.; Dresselhaus, M.S. Raman spectroscopy in graphene. *Phys. Rep.* **2009**, *473*, 51–87. [[CrossRef](#)]
8. Schwan, J.; Ulrich, S.; Batori, V.; Ehrhardt, H. Raman spectroscopy on amorphous carbon films. *J. Appl. Phys.* **1996**, *80*, 440. [[CrossRef](#)]
9. Tamor, M.A.; Vassell, W.C. Raman “fingerprinting” of amorphous carbon films. *J. Appl. Phys.* **1994**, *76*, 3823. [[CrossRef](#)]
10. Ferrari, A.C.; Rodil, S.E.; Robertson, J.; Milne, W.I. Is stress necessary to stabilise sp^3 bonding in diamond-like carbon? *Diam. Relat. Mater.* **2002**, *11*, 994–999. [[CrossRef](#)]
11. Irmer, G.; Dorner-Reisel, A. Micro-Raman Studies on DLC coatings. *Adv. Eng. Mater.* **2005**, *7*, 694–705. [[CrossRef](#)]
12. Calizo, I.; Balandin, A.A.; Bao, W.; Miao, F.; Lau, C.N. Temperature dependence of the Raman spectra of graphene and graphene multilayers. *Nano Lett.* **2007**, *7*, 2645–2649. [[CrossRef](#)] [[PubMed](#)]
13. Colombo, P.; Mera, G.; Riedel, R.; Soraru, G.D. Polymer-Derived Ceramics: 40 Years of Research and Innovation in Advanced Ceramics. *J. Am. Ceram. Soc.* **2010**, *93*, 1805–1837. [[CrossRef](#)]
14. Mera, G.; Navrotsky, A.; Sen, S.; Kleebe, H.; Riedel, R. Polymer-derived SiCN and SiOC ceramics—Structure and energetics at the nanoscale. *J. Mater. Chem. A* **2013**, *1*, 3826–3836. [[CrossRef](#)]
15. Linck, C.; Ionescu, E.; Papendorf, B.; Galuskova, D.; Galusek, D.; Šajgalík, P.; Riedel, R. Corrosion behavior of silicon oxycarbide-based ceramic nanocomposites under hydrothermal conditions. *Int. J. Mater. Res.* **2012**, *103*, 31–39. [[CrossRef](#)]
16. Modena, S.; Soraru, G.D.; Blum, Y.; Raj, R. Passive Oxidation of an Effluent System: The Case of Polymer-Derived SiCO. *J. Am. Ceram. Soc.* **2005**, *88*, 339–345. [[CrossRef](#)]
17. Ionescu, E.; Balan, C.; Kleebe, H.J.; Raj, R.; Müller, M.M.; Guillon, O.; Schliephake, D.; Heilmaier, M. High-Temperature Creep Behavior of SiOC Glass-Ceramics: Influence of Network Carbon Versus Segregated Carbon. *J. Am. Ceram. Soc.* **2014**, *97*, 3935–3942. [[CrossRef](#)]
18. Roth, F.; Schmerbauch, C.; Ionescu, E.; Raj, R.; Nicoloso, N.; Guillon, O. High-temperature piezoresistive C/SiOC sensors. *J. Sens. Sens. Syst.* **2015**, *4*, 133–136. [[CrossRef](#)]
19. Riedel, R.; Toma, L.; Janssen, E.; Hanselka, H.; Nuffer, J.; Melz, T. Piezoresistive Effect in SiOC Ceramics for Integrated Pressure Sensors. *J. Am. Ceram. Soc.* **2010**, *93*, 920–924. [[CrossRef](#)]

20. Graczyk-Zajac, M.; Reinold, L.M.; Kaspar, J.; Sasikumar, P.V.; Soraru, G.D.; Riedel, R. New Insights into Understanding Irreversible and Reversible Lithium Storage within SiOC and SiCN Ceramics. *Nanomaterials* **2015**, *5*, 233–245. [[CrossRef](#)] [[PubMed](#)]
21. Roth, F.; Waleska, P.; Hess, C.; Ionescu, E.; Nicoloso, N. UV Raman spectroscopy of segregated carbon in silicon oxycarbides. *J. Ceram. Soc. Jpn.* **2016**, *124*, 1042–1045. [[CrossRef](#)]
22. Cordelair, J.; Greil, P. Electrical conductivity measurements as a microprobe for structure transitions in polysiloxane derived Si–O–C ceramics. *J. Eur. Ceram. Soc.* **2000**, *20*, 1947–1957. [[CrossRef](#)]
23. Montagnac, G.; Caracas, R.; Bobocoiu, E.; Vittozb, F.; Reynarda, B. Anharmonicity of graphite from UV Raman spectroscopy to 2700 K. *Carbon* **2013**, *54*, 68–75. [[CrossRef](#)]
24. Linas, S.; Magnin, Y.; Poinso, B.; Boisron, O.; Förster, G.D.; Martinez, V.; Fulcrand, R.; Tournus, F.; Dupuis, V.; Rabilloud, F.; et al. Interplay between Raman shift and thermal expansion in graphene: Temperature-dependent measurements and analysis of substrate corrections. *Phys. Rev. B* **2015**, *91*, 075426. [[CrossRef](#)]
25. Zhang, X.; Yang, F.; Zhao, D.; Cai, L.; Luan, P.; Zhang, Q.; Zhou, W.; Zhang, N.; Fan, Q.X.; Wang, Y.; et al. Temperature dependent Raman spectra of isolated suspended single-walled carbon nanotubes. *Nanoscale* **2014**, *6*, 3949–3953. [[CrossRef](#)] [[PubMed](#)]
26. Ci, L.; Zhou, Z.; Song, L.; Yan, X.; Liu, D.; Yuan, H.; Gao, Y.; Wang, J.; Liu, L.; Zhou, W.; et al. Temperature dependence of resonant Raman scattering in double-wall carbon nanotubes. *Appl. Phys. Lett.* **2003**, *82*, 3098–3100. [[CrossRef](#)]
27. Koukaras, E.N.; Kalosakas, G.; Galiotis, C.; Papagelis, K. Phonon properties of graphene derived from molecular dynamics simulations. *Sci. Rep.* **2015**, *5*, 12923. [[CrossRef](#)] [[PubMed](#)]
28. Lindsay, L.; Broido, D.A. Optimized Tersoff and Brenner empirical potential parameters for lattice dynamics and phonon thermal transport in carbon nanotubes and graphene. *Phys. Rev. B* **2010**, *81*, 205441. [[CrossRef](#)]
29. Calizo, I.; Miao, F.; Bao, W.; Lau, C.N. Variable temperature Raman microscopy as a nanometrology tool for graphene layers and graphene-based devices. *Appl. Phys. Lett.* **2007**, *91*, 071913. [[CrossRef](#)]
30. Tan, P.; Deng, Y.; Zhao, Q. Temperature-dependent Raman spectra and anomalous Raman phenomenon of highly oriented pyrolytic graphite. *Phys. Rev. B* **1998**, *58*, 5435–5439. [[CrossRef](#)]
31. Raravikar, N.R.; Keblinski, P.; Rao, A.M.; Dresselhaus, M.S.; Schadler, L.S.; Ajayan, P.M. Temperature dependence of radial breathing mode Raman frequency of single-walled carbon nanotubes. *Phys. Rev. B* **2002**, *66*, 235424. [[CrossRef](#)]
32. Bassil, A.; Puech, P.; Tubery, L.; Bacsá, W. Controlled laser heating of carbon nanotubes. *Appl. Phys. Lett.* **2006**, *88*, 173113. [[CrossRef](#)]
33. Osswald, S.; Flahaut, E.; Gogotsi, Y. In Situ Raman Spectroscopy Study of Oxidation of Double- and Single-Wall Carbon Nanotubes. *Chem. Mater.* **2006**, *18*, 1525–1533. [[CrossRef](#)]
34. Baranov, A.V.; Bekhterev, A.N.; Bobovich, Y.S.; Petrov, V.I. Interpretation of certain characteristics in Raman spectra of graphite and glassy carbon. *Opt. Spectrosc.* **1987**, *62*, 612–616.
35. Thomsen, C.; Reich, S. Double resonant raman scattering in graphite. *Phys. Rev. Lett.* **2000**, *85*, 5214–5217. [[CrossRef](#)] [[PubMed](#)]
36. Vidano, R.; Fischbach, D.B. New Lines in the Raman Spectra of Carbons and Graphite. *J. Am. Ceram. Soc.* **1978**, *61*, 13–17. [[CrossRef](#)]
37. Nemanich, R.J.; Solin, S.A. First- and second-order Raman scattering from finite-size crystals of graphite. *Phys. Rev. B* **1979**, *20*, 392–401. [[CrossRef](#)]
38. Pimenta, M.A.; Dresselhaus, G.; Dresselhaus, M.S.; Cañado, L.G.; Jorio, A.; Saito, R. Studying disorder in graphite-based systems by Raman spectroscopy. *Phys. Chem. Chem. Phys.* **2007**, *9*, 1276–1291. [[CrossRef](#)] [[PubMed](#)]
39. Cañado, L.G.; Takai, K.; Enoki, T.; Endo, M.; Kim, Y.A.; Mizusaki, H. General equation for the determination of the crystallite size L_a of nanographite by Raman spectroscopy. *Appl. Phys. Lett.* **2006**, *88*, 163106. [[CrossRef](#)]
40. Ni, Z.H.; Fan, H.M.; Fan, X.F.; Wang, H.M.; Zheng, Z.; Feng, Y.P.; Wu, Y.H.; Shen, Z.X. High temperature Raman spectroscopy studies of carbon nanowalls. *J. Raman Spectrosc.* **2007**, *38*, 1449–1453. [[CrossRef](#)]
41. Tan, P.; Deng, Y.; Zhao, Q.; Cheng, W. The intrinsic temperature effect of the Raman spectra of graphite. *Appl. Phys. Lett.* **1999**, *74*, 1818–1820. [[CrossRef](#)]

42. Huang, F.; Yue, K.T.; Tan, P.; Zhang, S.-L. Temperature dependence of the Raman spectra of carbon nanotubes. *J. Appl. Phys.* **1998**, *84*, 4022. [[CrossRef](#)]
43. Bonini, N.; Lazzeri, M.; Marzari, N.; Mauri, F. Phonon anharmonicities in graphite and graphene. *Phys. Rev. Lett.* **2007**, *99*, 176802. [[CrossRef](#)] [[PubMed](#)]
44. Eckmann, A.; Felten, A.; Mishchenko, A.; Britnell, L.; Krupke, R.; Novoselov, K.S.; Casiraghi, C. Probing the nature of defects in graphene by Raman spectroscopy. *Nano Lett.* **2012**, *12*, 3925–3930. [[CrossRef](#)] [[PubMed](#)]



© 2018 by the authors. Licensee MDPI, Basel, Switzerland. This article is an open access article distributed under the terms and conditions of the Creative Commons Attribution (CC BY) license (<http://creativecommons.org/licenses/by/4.0/>).